HHS Public Access

Author manuscript

Radiother Oncol. Author manuscript; available in PMC 2018 May 02.

Published in final edited form as:

Radiother Oncol. 2017 May ; 123(2): 209–217. doi:10.1016/j.radonc.2017.04.006.

Regional Susceptibility to Dose-Dependent White Matter Damage After Brain Radiotherapy

Michael Connor, BS[a], **Roshan Karunamuni, PhD**[a,e], **Carrie McDonald, PhD**[a,c,e], **Tyler Seibert, MD, PhD**[a,e], **Nathan White, PhD**[b,e], **Vitali Moiseenko, PhD**[a], **Hauke Bartsch, PhD**[b,e], **Nikdokht Farid, MD**[b,e], **Joshua Kuperman, PhD**[b,e], **Anitha Krishnan, PhD**[b,e], **Anders Dale, PhD**[b,c,d,e], and **Jona Hattangadi-Gluth, MD**[a,e]

[a]Department of Radiation Medicine and Applied Sciences, University of California San Diego, United States

[b]Department of Radiology, University of California San Diego, United States

[c]Department of Psychiatry, University of California San Diego, United States

[d]Department of Neurosciences, University of California San Diego, United States

[e]Center for Multimodal Imaging and Genetics, University of California San Diego, United States

Abstract

Background and Purpose—Regional differences in sensitivity to white matter damage after brain radiotherapy (RT) are not well-described. We characterized the spatial heterogeneity of dose-response across white matter tracts using diffusion tensor imaging (DTI).

Materials and Methods—Forty-nine patients with primary brain tumors underwent MRI with DTI before and 9–12 months after partial-brain RT. Maps of fractional anisotropy (FA), mean diffusivity (MD), axial diffusivity (AD), and radial diffusivity (RD) were generated. Atlas-based white matter tracts were identified. A secondary analysis using skeletonized tracts was also performed. Linear mixed-model analysis of the relationship between mean and max dose and percent change in DTI metrics was performed.

Results—Tracts with the strongest correlation of FA change with mean dose were the fornix (−0.46 percent/Gy), cingulum bundle (−0.44 percent/Gy), and body of corpus callosum (−0.23 percent/Gy), $p<.001$. These tracts also showed dose-sensitive changes in MD and RD. In the skeletonized analysis, the fornix and cingulum bundle remained highly dose-sensitive. Maximum and mean dose were similarly predictive of DTI change.

Corresponding Author: Jona A. Hattangadi-Gluth, MD, Department of Radiation Medicine and Applied Sciences, 3855 Health Sciences Drive, La Jolla, CA 92093, jhattangadi@ucsd.edu, (858) 822-6040/(858) 246-1505 (fax).

Conflict of Interest Statement:

Dr. Hattangadi-Gluth has a research grant from Varian Medical Systems, unrelated to the current study. Dr. Dale receives funding through research agreements with General Electric Healthcare, and Medtronic, unrelated to the current study. Dr. Moiseenko reports prior honorarium and travel fees from Varian Medical Systems for a talk outside the submitted work.

Conclusions—The corpus callosum, cingulum bundle, and fornix show the most prominent dose-dependent changes following RT. Future studies examining correlation with cognitive functioning and potential avoidance of critical white matter regions are warranted.

Keywords

diffusion tensor imaging; white matter; Radiotherapy; dose-dependent; radiation

Introduction

Radiation therapy (RT) is standard of care for most primary and metastatic brain tumors. However, RT can damage healthy brain tissue, leading to neurocognitive deficits in verbal and nonverbal memory, executive function, and attention and problem-solving [1]. Pathogenesis of this process involves white matter damage driven by vascular injury, demyelination or axonal injury; parenchymal injury characterized by gliosis or neuroinflammation; impairment of hippocampal neural stem cell function; and possibly cortical thinning [2,3].

Despite advances in precision and conformality of RT delivery, there is little evidence regarding regional sensitivity of the brain to radiation on which to base applications of these technologies. There are no accepted regional dose constraints for white matter in fractionated partial brain RT. Maximum dose constraints exist for brain parenchyma in general, without distinguishing between cortex, white matter, and deep gray matter structures. Based on evidence that radiation impairs hippocampal neural stem cell differentiation [4], avoidance of the hippocampus during whole-brain RT for brain metastases has gained some traction and has been associated with improved memory preservation [5]. However, even without hippocampal damage, injury to its afferent and efferent white matter pathways may still result in memory decline or other cognitive impairment.

Radiation damage to white matter has been studied using diffusion tensor imaging (DTI), a non-invasive method of measuring the diffusion of water at the cellular level. DTI models the overall motion of water as an ellipsoid using a tensor model, with quantitative metrics allowing the study of white matter or axonal structures. Generally, DTI changes have been found to be progressive and occur after some threshold or in a dose-responsive manner [6–8]. Studies have generally focused on one or a few selected white matter regions. Pediatric patients have been found to have lower fractional anisotropy (more white matter disruption) in frontal lobe, temporal lobe, and periventricular white matter after radiation [9–11]. Other studies of adults have looked at only particular regions, such as the corpus callosum, parahippocampal cingulum, brain stem, and limbic circuit [8,12,13]. Many of these studies included patients receiving whole brain RT with a constant dose across the entire brain [9–13].

We previously analyzed DTI metrics of white matter damage after RT and found progressive, dose-dependent changes even at low doses and at time points early on after RT [14]. However, it is unclear which white matter regions of the brain are the most sensitive to radiation injury. Such insights would inform efforts towards cognitive-sparing RT. In this

study, we sought to characterize the spatial heterogeneity of dose-response to DTI metrics across white matter tracts using an atlas-based approach. The cohort consists of primary brain tumor patients receiving partial brain RT, to explore dose response and sensitivity across the entire white matter of the brain and across a range of probative doses.

Materials and Methods

Study Design

Study patients were treated with photon-based fractionated partial brain RT from January 2010 to December 2014. A total of 49 patients met criteria of MRI and DTI imaging [15] at pre-RT (or within one week of RT start) and one year post-RT (9–12 months) time points. Most patients were treated to 60 Gy in 30 fractions. Other dose schedules were converted to a total 30 fraction equivalent dose using biologically equivalent dose principles [16] and an α/β ratio of 2 Gy [14]. Treatment and demographic factors are shown in Supplementary Table 1. This study was approved by our institutional review board.

MRI Acquisition

MR imaging was performed on a 3T Signa Excite HDx scanner (GE Healthcare, Milwaukee, Wisconsin) equipped with an 8-channel head coil. The imaging protocol included a 3D volumetric T1-weighted inversion recovery spoiled gradient-echo sequence (echo time [TE]/ repetition time [TR] = 2.8/6.5 ms; inversion time [TI] = 450 ms; flip angle [FA] = 8 degrees; field of view [FOV] = 24 cm; 0.93 × 0.93 × 1.2 mm) and a 3D T2-weighted FLAIR sequence (TE/TR = 126/6000 ms; TI = 1863 ms; FOV = 24 cm; 0.93 × .093 × 1.2 mm). Diffusion data were acquired with a single-shot pulsed-field gradient spin-echo-planar imaging sequence (TE/TR = 96 ms/17 s; FOV = 24 cm, matrix = 128 × 128 × 48; slice thickness = 2.5 mm) at b = 0, 500, 1500, and 4000 s/mm^2, with 1, 6, 6, and 15 unique gradient directions for each b-value, respectively.

Image Processing and Registration

All image data were preprocessed using in-house algorithms developed in MATLAB (Mathworks, Natick, Massachusetts). Anatomical scans were corrected for distortions due to gradient nonlinearities using a spherical harmonic representation of the gradient fields [17]. Diffusion scans were corrected for spatial distortions associated with gradient nonlinearities, susceptibility (using a separate opposite phase-encoding polarity acquisition) [18], and eddy currents (using a post-acquisition correction algorithm) [19]. The diffusion tensor at each time point was calculated using mono-exponential fitting and data from all diffusion weightings (b=0, 500, 1000, 4000 s/mm^2). We analyzed four main diffusion metrics, each computed as a map at each time-point [14]. These diffusion metrics are defined in detail previously [14]: mean diffusivity (MD) represents the average mobility of water molecules and is sensitive to edema; fractional anisotropy (FA) is an expression of the degree of directional bias and hence a marker of microstructural white matter integrity; axial diffusivity (AD) represents diffusion along the white matter axon and is thought to be sensitive to axonal injury; radial diffusivity (RD) represents diffusion perpendicular to axonal orientation and is a marker of demyelination [20,21].

Weighted averages of T1 and T2 FLAIR images were calculated to account for edema and other pathology during registration of diffusion images. Pre-RT MRI images were linearly co-registered to the CT simulation images used in radiation treatment planning. The quality of this registration was confirmed visually slice-by-slice, and the resulting transformation matrix was used to resample the delivered radiation dose distribution to the MRI volume space. To avoid bias to one time point [22], MRI volumes from each time point were non-linearly registered to the MNI152 standard-space T1-weighted average structural template image, a normal brain atlas, using FSL's FNIRT, a standard nonlinear registration algorithm which implements a "sum-of-squared differences" cost function [23,24]. Tumor and surgical beds/scars were censored from consideration during the registration [3,14]. Successful registration was confirmed via visual inspection. The resulting deformation fields were applied to the diffusion images and pre-RT dose map.

Regions of Interest Analysis

With all patient diffusion scans in MNI space, regions of interest were defined using ICBM-DTI-81 white-matter labels atlas [25]. Paired structures were considered as two observations of one region. Twenty-one ROIs were identified. Representative tracts are shown and labeled in Figure 1. A censoring mask including tumor, tumor bed, surgical cavity, surgical scars, and any T2 FLAIR edema hyperintensity was manually drawn for each patient and for each time point separately. To guard against the inclusion of non-white matter due to small registration errors or misalignment of the ICBM-DTI-81 hand-drawn labels with our actual subject anatomy, we excluded voxels with a baseline FA of less than 0.2 on the basis these may not represent well-defined white matter tracts [26].

Skeletonized Analysis

Skeletonization of white matter tracts, as with FSL's Tract-Based Spatial Statistics, is a common method of aligning FA images from multiple subjects via projection onto an alignment-invariant tract representation (the "mean FA skeleton") [26]. This process may compensate for local registration errors and improve the sensitivity, objectivity and interpretability of analysis of multi-subject diffusion imaging studies [27]. We undertook a secondary analysis of skeletonized white matter tracts to determine if our findings were reproducible with this method.

A mean of the FA images of all subjects was created and thinned to create a mean FA skeleton which represents the centers of all tracts common to the group. Each subject's aligned FA data was then projected onto this skeleton by assigning the maximum FA value perpendicular to the skeleton to the nearest skeleton voxel [26]. The same projections were also applied to all MD, AD, and RD maps to generate skeletonized forms of these maps as well.

Statistical Analysis

Mean dose ranges to each tract are shown in Supplementary Figure 1, and voxel size of each tract pre- and post-RT is shown in Supplementary Table 2. Mean values for MD, FA, AD, and RD were obtained for each region of interest. We used R [28] and *lme4* [29] to perform linear mixed effects analyses fit using maximum likelihood. Percent change from baseline to

post-RT for each DTI metric was chosen as the dependent variable. A dose (continuous variable, mean dose and max dose) by tract (categorical variable) interaction was included as a fixed effect. To control for correlated observations within subjects, we tested a subject-specific random intercept. Model selection was based on likelihood ratio tests of the full model above versus reduced models. To correct for multiple comparisons, the p-values for univariate, region-specific slopes (obtained based on restricted maximum likelihood) were adjusted by Bonferroni correction. Regions with significant radiation dose-dependent change in DTI metrics after adjustment were identified, defined as adjusted p-value < 0.05.

Results

Region of interest analyses of white matter dose sensitivity with model coefficients (representing percent change per Gy for mean and maximum dose) and p-values are shown in Table 1. These data are graphically represented in Figure 2. Decreases in FA connote white matter disruption. For correlation with mean dose, the white matter tracts most dose-sensitive to decreases in FA were the column and body of fornix (−0.46 percent per Gy, p<.001), cingulum bundle (−0.44 percent per Gy, p<.001), and body of corpus callosum (−0.23 percent per Gy, p<.001). For MD, the column and body of fornix, cingulum bundle, tapetum, and genu and body of the corpus callosum were among the ROIs to show the most dose sensitivity (p<.001), Table 1, Figure 2. These structures were similarly associated with significant dose-dependent increase in RD as well. The posterior limb of the internal capsule experienced dose-dependent increase in FA, decrease in MD and decrease in RD (Table 1). With rare exception, correlations with mean and max dose were either both significant or both not significant with similar coefficients. Decrease in FA and increase in MD were dose-dependent in the splenium for maximum dose but not mean dose. Regions with statistically significant dose dependency are shown superimposed on the MNI atlas in Figure 4. Greatest dose sensitivity was observed in central limbic structures.

In the secondary analysis performed on skeletonized white matter tracts, the column and body of fornix (−0.32 percent per Gy, p<.001) and cingulum bundle (−0.29 percent per Gy, p<.001) again showed significant dose-dependent decrease in FA. The full results for this analysis are shown in Table 2 and Figure 3.

Discussion

In this tract-based analysis of regional white matter damage after fractionated brain RT, we found strongest dose-dependence within the corpus callosum, fornix, and cingulum bundle. These regions exhibited dose-dependent increases in RD and MD and decreases in FA, suggesting demyelination and loss of axonal integrity with progressive dose. Elucidation of regional white matter sensitivity within the context of neural networks of memory and higher-order cognition is critical to understanding the pathogenesis of radiation-induced cognitive decline, as well as informing studies on cognitive-sparing RT. The white matter regions identified in the current study have close interplay with the hippocampal network and association cortex that also appear to be dose-sensitive [30,31], supporting the idea that damage within these networks may mediate the neurocognitive sequelae of brain radiotherapy.

Pronounced dose-dependent changes were seen in the dorsal component of the cingulum bundle. Though nuanced portions and connections of the cingulum bundle are still being elucidated [32], in general this white matter structure projects from the cingulate gyrus to the entorhinal cortex. The dorsal cingulum has widespread connections with the frontal lobe, playing a role in attention, volitional control of cognition, and emotion. The ventral cingulum, or parahippocampal component, is involved in visuospatial processing and verbal memory [33]. Changes in the cingulum bundle are observed in many conditions such as traumatic brain injury, mild cognitive impairment (MCI), and Alzheimer's [32]. Cognitive control in older adults is very sensitive to cingulum microstructure [34]. In patients with MCI, changes within the ventral cingulum are predictive of (and detectable prior to) hippocampal volume loss and memory performance [35]. While a previous study of radiation effects on white matter found dose sensitivity to DTI changes in the parahippocampal cingulum [36], we did not detect robust dose-sensitivity in this structure. Indeed the distinction between the dorsal and ventral aspects of the cingulum are rather arbitrary, and may vary by DTI atlas [25,32]. In our DTI atlas, the parahippocampal cingulum is smaller, just the projections within the parahippocampal gyrus, thus changes within this structure may be more influenced by partial voluming (for example by increases in cerebrospinal fluid). Given our strict exclusion criteria and methodology which excluded "non-white matter" voxels with FA<0.2, we may have been underpowered to detect dose-dependent changes in the parahippocampal cingulum.

Increased vulnerability to dose-dependent change was also detected in the fornix. The fornices originate from the bilateral hippocampi, merge at midline, and again diverge to the septal nuclei, nucleus accumbens, and hypothalamus. An essential element of the limbic circuit, injury or transection of the fornix is associated with memory loss, particularly in episodic memory [37], which is the most common deficit seen after brain radiotherapy [38]. Studies have implicated the fornix as the site of the earliest and most robust changes in Alzheimer's disease [37]. While there has been intense focus on the effect of radiation on the hippocampus [4] with hippocampal-sparing RT evaluated in nationwide clinical trials [5,39], the associated white matter regions within the hippocampal network have largely been ignored. This is the first study to show exquisite radiation dose sensitivity in the fornix, the key afferent pathway from the hippocampus, suggesting that dose-dependent damage to the fornix may contribute to impairment of the hippocampal network.

The corpus callosum facilitates communication between the left and right sides of the brain. It consists of the genu and rostrum anteriorly, the splenium posteriorly, and the body in between [33]. Lesion or transection, depending on the specific anatomical localization, may lead to reduced processing speed, difficulty with visuospatial processing, dysnomia, and other cognitive impairments [33]. Alterations in corpus callosum microstructure have been shown to correlate with age-related reductions in processing speed [40], and are associated with other cognitive disorders such as MCI, traumatic brain injury, and Alzheimer's [41–43].

Our findings concur with a prior study of radiation damage to white matter after whole-brain RT (WBRT) at doses of 30 or 37.5 Gy [44]. In that WBRT study, the greatest DTI changes were seen, in descending order, in the inferior cingula, body of corpus callosum, and fornix. While this is similar to what we have found here, we were able to demonstrate dose-

dependent white matter damage by analyzing various tracts that received a wide range of doses. These complementary studies suggest that the white matter regions highlighted are most vulnerable to radiation damage, and our results, over a wider range of doses, suggest they may be susceptible to damage even after low-dose radiation exposure. The clinical significance of this requires further study. The use of a wider range of diffusion weightings in the current study may yield a diffusion tensor more robust to variation in white matter microstructure [14,15].

With respect to dose, a recent DTI study found that elongated white matter tracts after partial brain RT responded more to maximum dose rather than mean dose [36]. The possibility of serial structure response carries important implications for RT planning, as this suggests that limiting hot spots within a tract is more important than limiting the mean dose delivered to the entire structure. Our results showed no difference in DTI outcomes using mean or maximum dose as the predictor of white matter damage. This discrepancy warrants further exploration.

Although neurocognitive outcomes were not available for the patients in this study, the tracts identified as particularly radiation sensitive are known to correlate with cognitive decline in other diseases. Thus, the radiation-induced white matter damage described in our study has a potential role in radiation-induced cognitive dysfunction. The fornix and cingulum bundle are elements of the limbic system, an interconnected circuit including the hippocampus which regulate emotion, memory and learning, behavior, and attention [45]. Implicated in a range of disorders featuring cognitive dysfunction from MCI to Alzheimer's and major depression to schizophrenia [46,47], the limbic system has been investigated as a specifically sensitive structure in whole-brain RT studies [13,44]. Indeed, brain RT patients experience cognitive dysfunction similar to that of other disorders where damage to limbic structures is believed to play a role.

There has been speculation that fibers that myelinate later in development are more susceptible to injury than those developing first, a hypothesis known as retrogenesis [48]. The limbic and commissural pathways are among the last to myelinate [49] and indeed were identified in this study as having the most pronounced dose-dependent response to radiation. Consistent with studies of other white matter pathologies, early-myelinating tracts such as the internal capsule or corticospinal tract were less sensitive [48]. The structures we identified are also deep or periventricular white matter, perhaps implicating decreased perfusion as a potential contributor [44,50].

Limitations to our study include its retrospective nature and potential confounding effects of systemic therapy, tumor effects, surgical sequelae, or other factors affecting white matter structure or integrity. Registration inaccuracy is always a concern in diffusion MRI, and we have mitigated this concern by careful visual inspection and excluding voxels with a FA less than 0.2. We also repeated the analysis on skeletonized white matter tracts which showed retained significance for the fornix and cingulum. The corpus callosum lost significance in the skeletonized analysis, which suggests there could have been some registration issues in this region. We detected a counter-intuitive, dose-dependent increase in FA, or decrease in RD, in a couple of instances. A possible cause of this include undetected resolution of

edema not evident on imaging for censoring [51]. The posterior limb of the internal capsule, did, interestingly, have the highest baseline FA in our study (0.58 for ROI-based analysis, 0.74 for skeletonized analysis). It is possible that these tightly-packed tracts were more susceptible to mechanisms known to cause FA increase. For example, several studies have demonstrated increased FA in traumatic brain injury (TBI) likely due to axonal swelling [52]. Additionally, compression of brain tissue caused by tumor mass effect can also cause increased FA in peri-tumoral white matter [53], and these effects may be preferentially seen in tightly-packed, more organized white matter. Increase in FA can also be observed in areas of crossing fibers as damage to these regions results in less crossing, and actually greater anisotropy. A prior study concluded that increased fiber crossing and interaction with other WM tracts, such as the interhemispheric projections, resulted in paradoxical results in corticospinal tracts [54]. Finally, astrogliosis with compaction of axonal neurofilaments could result in increased FA [55,56].

Our study lacks histopathological outcomes, though preclinical data show a correlation between changes in diffusivity metrics and white matter damage [20]. Given that radiation damage evolves over several years, future studies should examine effects at longer follow-up after RT. The precise relationship between the changes observed here and cognitive decline is unclear. Studies correlating the changes seen here with post-RT cognitive decline are underway at our institution.

Conclusions

Among white matter tracts, we detected the most prominent dose-dependent changes after RT in the corpus callosum, cingulum bundle, and fornix. Susceptibility to radiation-induced white matter damage may follow patterns seen in other cognitive disorders such as the retrogenesis model in Alzheimer's disease. This may support future study into dose-sparing protocols for avoidance of not only the hippocampus, but of associated white matter structures that may contribute to cognitive decline.

Supplementary Material

Refer to Web version on PubMed Central for supplementary material.

Acknowledgments

None

Funding: This work was partially supported by the following grants: National Institutes of Health (KL2RR031978, KL2TR00099, UL1TR000100 to J.H-G.); American Cancer Society (Pilot Award ACS-IRG #70-002 to J.H-G.); National Science Foundation Grant (1430082 to N.W.); American Cancer Society Research (Scholar Grant RSG-15-229-01-CCE to C.M.); National Cancer Institute Cancer Center (Specialized Grant P30CA023100 to C.M., J.H-G.) No study sponsor was directly involved in study design; in the collection, analysis and interpretation of data; in the writing of the manuscript; or in the decision to submit the manuscript for publication.

References

1. Crossen JR, Garwood D, Glatstein E, Neuwelt EA. Neurobehavioral sequelae of cranial irradiation in adults: a review of radiation-induced encephalopathy. J Clin Oncol. 1994; 12:627–42. [PubMed: 8120563]

2. Greene-Schloesser D, Robbins ME, Peiffer AM, Shaw EG, Wheeler KT, Chan MD. Radiation-induced brain injury: A review. Front Oncol. 2012; 2:1–18. DOI: 10.3389/fonc.2012.00073

3. Karunamuni R, Bartsch H, White NS, Moiseenko V, Carmona R, Marshall DC, et al. Dose-Dependent Cortical Thinning after Partial Brain Irradiation in High-Grade Glioma. Int J Radiat Oncol Biol Phys. 2016; 94:297–304. DOI: 10.1016/j.ijrobp.2015.10.026 [PubMed: 26853338]

4. Monje ML, Mizumatsu S, Fike JR, Palmer TD. Irradiation induces neural precursor-cell dysfunction. Nat Med. 2002; 8:955–62. DOI: 10.1038/nm749 [PubMed: 12161748]

5. Gondi V, Pugh SL, Tome WA, Caine C, Corn B, Kanner A, et al. Preservation of Memory With Conformal Avoidance of the Hippocampal Neural Stem-Cell Compartment During Whole-Brain Radiotherapy for Brain Metastases (RTOG 0933): A Phase II Multi-Institutional Trial. J Clin Oncol. 2014; 32:3810–6. DOI: 10.1200/JCO.2014.57.2909 [PubMed: 25349290]

6. Haris M, Kumar S, Raj MK, Das KJM, Sapru S, Behari S, et al. Serial diffusion tensor imaging to characterize radiation-induced changes in normal-appearing white matter following radiotherapy in patients with adult low-grade gliomas. Radiat Med - Med Imaging Radiat Oncol. 2008; 26:140–50. DOI: 10.1007/s11604-007-0209-4

7. Ravn S, Holmberg M, Sørensen P, Frøkjær JB, Carl J. Differences in supratentorial white matter diffusion after radiotherapy–new biomarker of normal brain tissue damage? Acta Oncol (Madr). 2013; 52:1314–9. DOI: 10.3109/0284186X.2013.812797

8. Nagesh V, Tsien CI, Chenevert TL, Ross BD, Lawrence TS, Junick L, et al. Radiation-Induced Changes in Normal-Appearing White Matter in Patients With Cerebral Tumors: A Diffusion Tensor Imaging Study. Int J Radiat Oncol Biol Phys. 2008; 70:1002–10. DOI: 10.1016/j.ijrobp.2007.08.020 [PubMed: 18313524]

9. Qiu D, Kwong DLW, Chan GCF, Leung LHT, Khong P-L. Diffusion Tensor Magnetic Resonance Imaging Finding of Discrepant Fractional Anisotropy Between the Frontal and Parietal Lobes After Whole-Brain Irradiation in Childhood Medulloblastoma Survivors: Reflection of Regional White Matter Radiosensitivity? Int J Radiat Oncol. 2007; 69:846–51. DOI: 10.1016/j.ijrobp.2007.04.041

10. Dellani PR, Eder S, Gawehn J, Vucurevic G, Fellgiebel A, Müller MJ, et al. Late structural alterations of cerebral white matter in long-term survivors of childhood leukemia. J Magn Reson Imaging. 2008; 27:1250–5. DOI: 10.1002/jmri.21364 [PubMed: 18504742]

11. Leung LHT, Ooi GC, Kwong DLW, Chan GCF, Cao G, Khong PL. White-matter diffusion anisotropy after chemo-irradiation: A statistical parametric mapping study and histogram analysis. Neuroimage. 2004; 21:261–8. DOI: 10.1016/j.neuroimage.2003.09.020 [PubMed: 14741664]

12. Welzel T, Niethammer A, Mende U, Heiland S, Wenz F, Debus J, et al. Diffusion tensor imaging screening of radiation-induced changes in the white matter after prophylactic cranial irradiation of patients with small cell lung cancer: first results of a prospective study. AJNR Am J Neuroradiol. 2008; 29:379–83. DOI: 10.3174/ajnr.A0797 [PubMed: 17974610]

13. Nazem-Zadeh M-R, Chapman CH, Lawrence TL, Tsien CI, Cao Y. Radiation therapy effects on white matter fiber tracts of the limbic circuit. Med Phys. 2012; 39:5603.doi: 10.1118/1.4745560 [PubMed: 22957626]

14. Connor M, Karunamuni R, McDonald C, White N, Pettersson N, Moiseenko V, et al. Dose-dependent white matter damage after brain radiotherapy. Radiother Oncol. 2016; doi: 10.1016/j.radonc.2016.10.003

15. White NS, Leergaard TB, D'Arceuil H, Bjaalie JG, Dale AM. Probing tissue microstructure with restriction spectrum imaging: Histological and theoretical validation. Hum Brain Mapp. 2013; 34:327–46. DOI: 10.1002/hbm.21454 [PubMed: 23169482]

16. Bruzzaniti V, Abate A, Pedrini M, Benassi M, Strigari L. IsoBED: a tool for automatic calculation of biologically equivalent fractionation schedules in radiotherapy using IMRT with a simultaneous integrated boost (SIB) technique. J Exp Clin Cancer Res. 2011; 30:52.doi: 10.1186/1756-9966-30-52 [PubMed: 21554675]

17. Jovicich J, Czanner S, Greve D, Haley E, Van Der Kouwe A, Gollub R, et al. Reliability in multi-site structural MRI studies: Effects of gradient non-linearity correction on phantom and human data. Neuroimage. 2006; 30:436–43. DOI: 10.1016/j.neuroimage.2005.09.046 [PubMed: 16300968]

18. Holland D, Kuperman JM, Dale AM. Efficient Correction of Inhomogeneous Static Magnetic Field- Induced Distortion in Echo Planar Imaging. Neuroimage. 2011; 50:1–18. DOI: 10.1016/j.neuroimage.2009.11.044.Efficient
19. Zhuang J, Hrabe J, Kangarlu A, Xu D, Bansal R, Branch CA, et al. Correction of eddy-current distortions in diffusion tensor images using the known directions and strengths of diffusion gradients. J Magn Reson Imaging. 2006; 24:1188–93. DOI: 10.1002/jmri.20727 [PubMed: 17024663]
20. Song S-K, Sun S-W, Ramsbottom MJ, Chang C, Russell J, Cross AH. Dysmyelination Revealed through MRI as Increased Radial (but Unchanged Axial) Diffusion of Water. Neuroimage. 2002; 17:1429–36. DOI: 10.1006/nimg.2002.1267 [PubMed: 12414282]
21. Alexander AL, Lee JE, Lazar M, Field AS. Diffusion tensor imaging of the brain. Neurotherapeutics. 2007; 4:316–29. DOI: 10.1016/j.nurt.2007.05.011 [PubMed: 17599699]
22. Reuter M, Fischl B. Avoiding asymmetry-induced bias in longitudinal image processing. Neuroimage. 2011; 57:19–21. DOI: 10.1016/j.neuroimage.2011.02.076 [PubMed: 21376812]
23. Fischl B, Salat DH, Busa E, Albert M, Dieterich M, Haselgrove C, et al. Whole brain segmentation: Automated labeling of neuroanatomical structures in the human brain. Neuron. 2002; 33:341–55. DOI: 10.1016/S0896-6273(02)00569-X [PubMed: 11832223]
24. Andersson JLR, Jenkinson M, Smith S. Non-linear registration aka Spatial normalisation. FMRIB Technial Report TR07JA2. 2007:22.
25. Mori S, Oishi K, Jiang H, Jiang L, Li X, Akhter K, et al. Stereotaxic white matter atlas based on diffusion tensor imaging in an ICBM template. Neuroimage. 2008; 40:570–82. DOI: 10.1016/j.neuroimage.2007.12.035 [PubMed: 18255316]
26. Smith SM, Jenkinson M, Johansen-Berg H, Rueckert D, Nichols TE, Mackay CE, et al. Tract-based spatial statistics: Voxelwise analysis of multi-subject diffusion data. Neuroimage. 2006; 31:1487–505. DOI: 10.1016/j.neuroimage.2006.02.024 [PubMed: 16624579]
27. Schwarz C, Reid R, Kantarci K, Jack CR Jr. Improved DTI registration alows voxel-based analysis that outperforms Tract-based Spatial Statistics. Neuroimage. 2012; 29:997–1003. DOI: 10.1016/j.biotechadv.2011.08.021
28. R Core Team. R: A Language and Environment for Statistical Computing. Vienna, Australia: 2015. https://www.r-project.org n.d.
29. Bates D, Mächler M, Bolker B, Walker S. Fitting Linear Mixed-Effects Models Using **lme4**. J Stat Softw. 2015; 67doi: 10.18637/jss.v067.i01
30. Seibert TM, Karunamuni R, Bartsch H, Kaifi S, Krishnan A, Dalia Y, et al. Radiation dose-dependent hippocampal atrophy detected with longitudinal volumetric MRI. Int J Radiat Oncol. 2016; doi: 10.1016/j.ijrobp.2016.10.035
31. Seibert TM, Karunamuni R, Kaifi S, Burkeen J, Krishnan A, McDonald C, et al. Selective Vulnerability of Cerebral Cortex Regions to Radiation Dose-Dependent Atrophy. Int J Radiat Oncol. 2016; 96:S177.doi: 10.1016/J.IJROBP.2016.06.445
32. Jones DK, Christiansen KF, Chapman RJ, Aggleton JP. Distinct subdivisions of the cingulum bundle revealed by diffusion MRI fibre tracking: Implications for neuropsychological investigations. Neuropsychologia. 2013; 51:67–78. DOI: 10.1016/j.neuropsychologia.2012.11.018 [PubMed: 23178227]
33. Maheshwari, M., Klein, A., Ulmer, JL. Funct Neuroradiol. Boston, MA: Springer US; 2011. White Matter: Functional Anatomy of Key Tracts; p. 767-83.
34. Metzler-Baddeley C, Jones DK, Steventon J, Westacott L, Aggleton JP, O'Sullivan MJ. Cingulum microstructure predicts cognitive control in older age and mild cognitive impairment. J Neurosci. 2012; 32:17612–9. DOI: 10.1523/JNEUROSCI.3299-12.2012 [PubMed: 23223284]
35. Delano-Wood L, Stricker NH, Sorg SF, Nation DA, Jak AJ, Woods SP, et al. Posterior cingulum white matter disruption and its associations with verbal memory and stroke risk in mild cognitive impairment. J Alzheimers Dis. 2012; 29:589–603. DOI: 10.3233/JAD-2012-102103 [PubMed: 22466061]
36. Zhu T, Chapman CH, Tsien C, Kim M, Spratt DE, Lawrence TS, et al. Effect of the Maximum Dose on White Matter Fiber Bundles Utilizing Longitudinal Diffusion Tensor Imaging. Int J Radiat Oncol. 2016; doi: 10.1016/j.ijrobp.2016.07.010

37. Oishi K, Lyketsos CG. Alzheimer's disease and the fornix. Front Aging Neurosci. 2014; 6:1–9. DOI: 10.3389/fnagi.2014.00241 [PubMed: 24478697]
38. Meyers CA, Brown PD. Role and relevance of neurocognitive assessment in clinical trials of patients with CNS tumors. J Clin Oncol. 2006; 24:1305–9. DOI: 10.1200/JCO.2005.04.6086 [PubMed: 16525186]
39. Sidney Kimmel Comprehensive Cancer Center. Hippocampal Prophylactic Cranial Irradiation for Small Cell Lung Cancer - Full Text View - ClinicalTrials.gov n.d. https://clinicaltrials.gov/show/NCT01797159
40. Kerchner GA, Racine CA, Hale S, Wilheim R, Laluz V, Miller BL, et al. Cognitive Processing Speed in Older Adults: Relationship with White Matter Integrity. PLoS One. 2012; 7doi: 10.1371/journal.pone.0050425
41. Stricker NH, Salat DH, Kuhn TP, Foley JM, Price JS, Westlye LT, et al. Mild Cognitive Impairment is Associated With White Matter Integrity Changes in Late-Myelinating Regions Within the Corpus Callosum. Am J Alzheimers Dis Other Demen. 2016; 31:68–75. DOI: 10.1177/1533317515578257 [PubMed: 25904759]
42. Ubukata S, Ueda K, Sugihara G, Yassin W, Aso T, Fukuyama H, et al. Corpus Callosum Pathology as a Potential Surrogate Marker of Cognitive Impairment in Diffuse Axonal Injury. J Neuropsychiatry Clin Neurosci. 2016; 28:97–103. DOI: 10.1176/appi.neuropsych.15070159 [PubMed: 26569151]
43. Di Paola M, Spalletta G, Caltagirone C. In vivo structural neuroanatomy of corpus callosum in Alzheimer's disease and mild cognitive impairment using different MRI techniques: A review. J Alzheimer's Dis. 2010; 20:67–95. DOI: 10.3233/JAD-2010-1370 [PubMed: 20164572]
44. Chapman CH, Nazem-Zadeh M, Lee OE, Schipper MJ, Tsien CI, Lawrence TS, et al. Regional Variation in Brain White Matter Diffusion Index Changes following Chemoradiotherapy: A Prospective Study Using Tract-Based Spatial Statistics. PLoS One. 2013; 8doi: 10.1371/journal.pone.0057768
45. Rajmohan V, Mohandas E. The limbic system. Indian J Psychiatry. 2007; 49:132–9. DOI: 10.4103/0019-5545.33264 [PubMed: 20711399]
46. Mori S, Aggarwal M. In vivo magnetic resonance imaging of the human limbic white matter. Front Aging Neurosci. 2014; 6:1–6. DOI: 10.3389/fnagi.2014.00321 [PubMed: 24478697]
47. Hoogenboom WS, Perlis RH, Smoller JW, Zeng-Treitler Q, Gainer VS, Murphy SN, et al. Limbic system white matter microstructure and long-term treatment outcome in major depressive disorder: a diffusion tensor imaging study using legacy data. World J Biol Psychiatry. 2014; 15:122–34. DOI: 10.3109/15622975.2012.669499 [PubMed: 22540406]
48. Stricker NH, Schweinsburg BC, Delano-Wood L, Wierenga CE, Bangen KJ, Haaland KY, et al. Decreased white matter integrity in late-myelinating fiber pathways in Alzheimer's disease supports retrogenesis. Neuroimage. 2009; 45:10–6. DOI: 10.1016/j.neuroimage.2008.11.027 [PubMed: 19100839]
49. Kinney H, Brody B, Kloman A, Gilles F. Sequence of central nervous system myelination in human infancy: II. An autopsy study of myelination. J Neuropathol Exp Neurol. 1988; 46:283–301. DOI: 10.1097/00005072-198705000-00005
50. Khong P. White Matter Anisotropy in Post-Treatment Childhood Cancer Survivors: Preliminary Evidence of Association With Neurocognitive Function. J Clin Oncol. 2006; 24:884–90. DOI: 10.1200/JCO.2005.02.4505 [PubMed: 16484697]
51. Armitage PA, Bastin ME, Marshall I, Wardlaw JM, Cannon J. Diffusion anisotropy measurements in ischaemic stroke of the human brain. MAGMA. 1998; 6:28–36. [PubMed: 9794287]
52. Roberts RM, Mathias JL, Rose SE. Diffusion Tensor Imaging (DTI) findings following pediatric non-penetrating TBI: a meta-analysis. Dev Neuropsychol. 2014; 39:600–37. DOI: 10.1080/87565641.2014.973958 [PubMed: 25470224]
53. Chenevert TL, Ross BD. Diffusion imaging for therapy response assessment of brain tumor. Neuroimaging Clin N Am. 2009; 19:559–71. DOI: 10.1016/j.nic.2009.08.009 [PubMed: 19959005]

54. Rose SE, Hatzigeorgiou X, Strudwick MW, Durbridge G, Davies PSW, Colditz PB. Altered white matter diffusion anisotropy in normal and preterm infants at term-equivalent age. Magn Reson Med. 2008; 60:761–7. DOI: 10.1002/mrm.21689 [PubMed: 18816850]

55. Croall ID, Cowie CJA, He J, Peel A, Wood J, Aribisala BS, et al. White matter correlates of cognitive dysfunction after mild traumatic brain injury. Neurology. 2014; 83:494–501. DOI: 10.1212/WNL.0000000000000666 [PubMed: 25031282]

56. Budde MD, Janes L, Gold E, Turtzo LC, Frank JA. The contribution of gliosis to diffusion tensor anisotropy and tractography following traumatic brain injury: Validation in the rat using Fourier analysis of stained tissue sections. Brain. 2011; 134:2248–60. DOI: 10.1093/brain/awr161 [PubMed: 21764818]

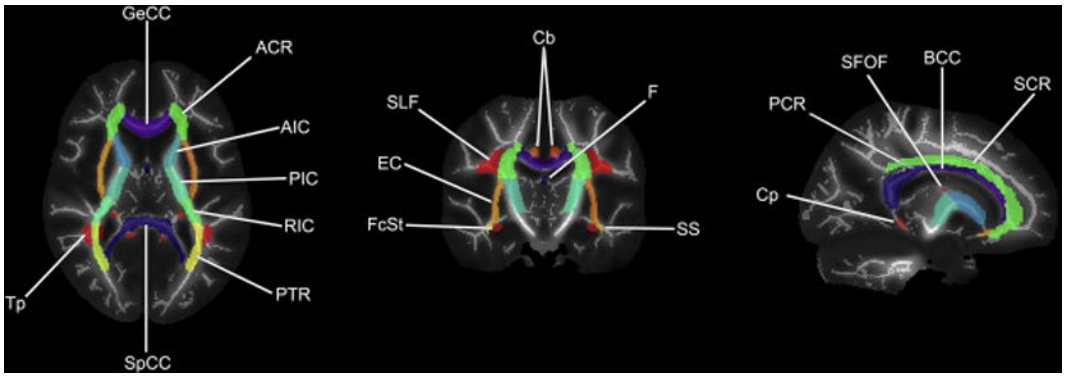

Fig 1.

Representative JHU ICBM-DTI-81 white-matter atlas labels overlaid on our cohort's mean FA image and mean FA skeleton. GeCC, genu of corpus callosum; ACR, anterior corona radiata; AIC, anterior limb of internal capsule; PIC, posterior limb of internal capsule; RIC, rentrolenticular part of internal capsule; PTR, posterior thalamic radiation; SpCC, splenium of corpus callosum; Tp, tapetum; FcSt, fornix (cres)/stria terminalis; EC, external capsule; SLF, superior longitudinal fasciculus; Cb, cingulum bundle ; F, fornix (column and body of fornix); SS, sagittal stratum; Cp, cingulum (parahippocampal); PCR, posterior corona radiate; SFOF, superior fronto-occipital fasciculus; BCC, body of corpus callosum; SCR, superior corona radiata. Note: uncinate fasciculus and corticospinal tracts not shown.

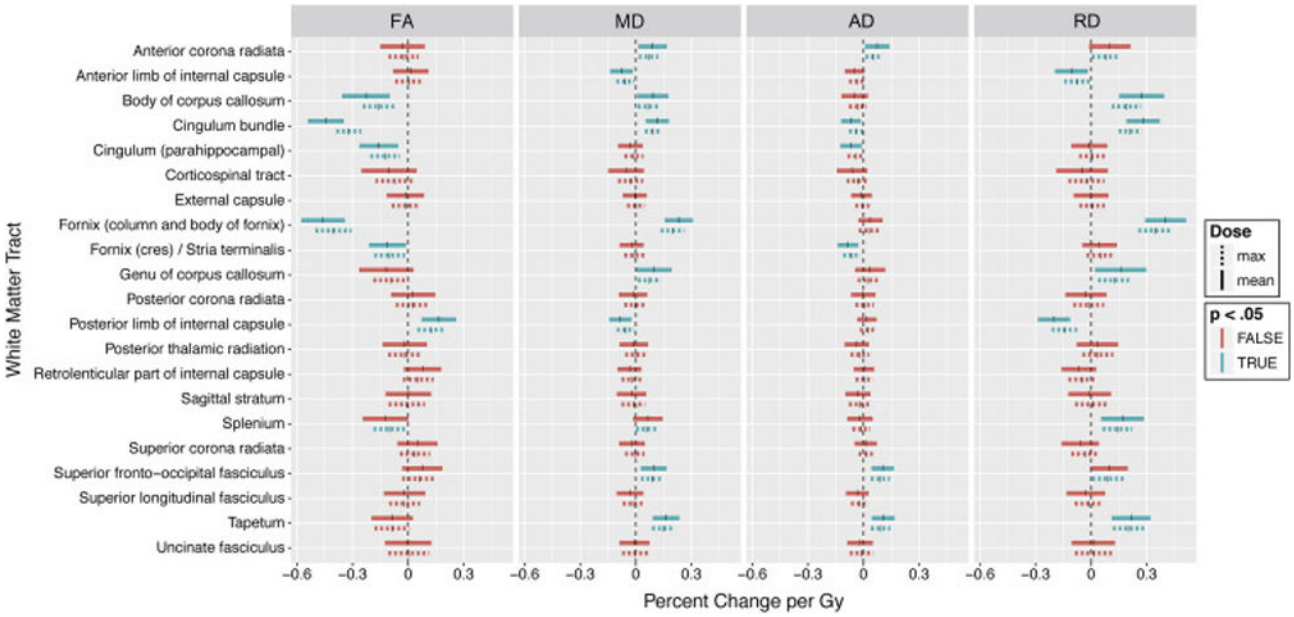

Fig 2.

Linear mixed model coefficients; whole ROI analysis. Vertical ticks represent percent change per Gy. Shaded widths are 95% confidence intervals adjusted for multiple comparisons. Statistical significance ($p<.05$, Bonferroni adjusted for n=21) is color-coded. Solid lines are correlations with mean dose; dashed lines are correlations with maximum dose.

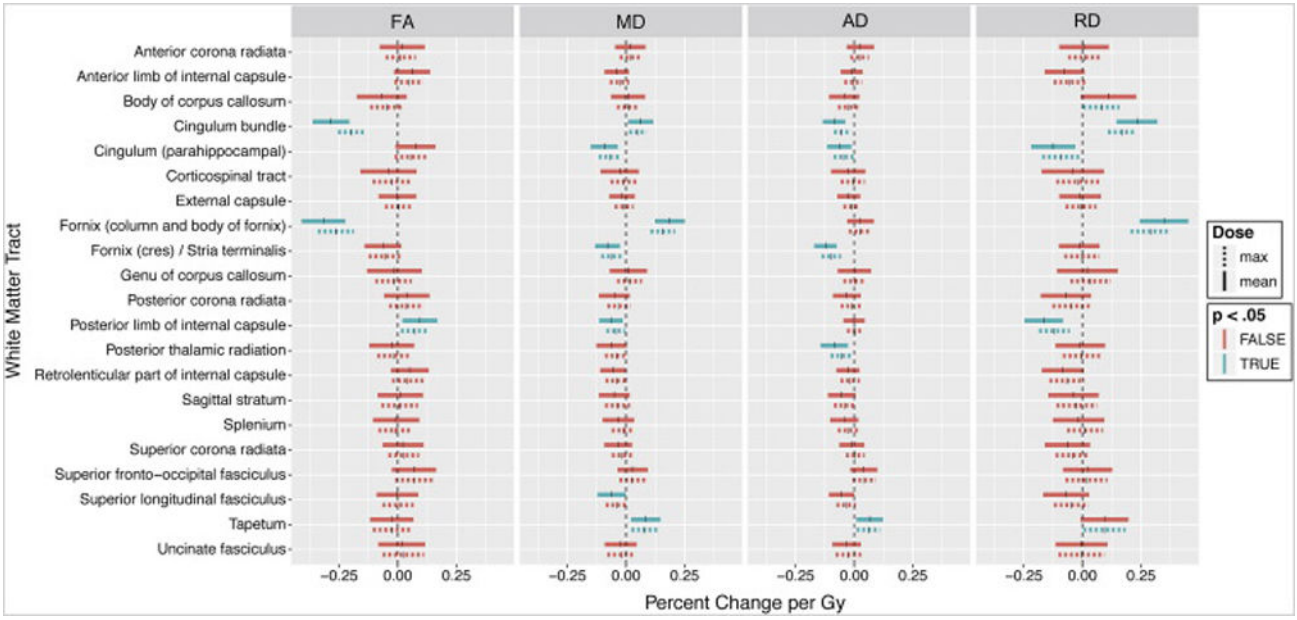

Fig 3.

Linear mixed model coefficients; skeletonized tract analysis. Vertical ticks represent percent change per Gy. Shaded widths are 95% confidence intervals adjusted for multiple comparisons. Statistical significance ($p<.05$, Bonferroni adjusted for n=21) is color-coded. Solid lines are correlations with mean dose; dashed lines are correlations with maximum dose.

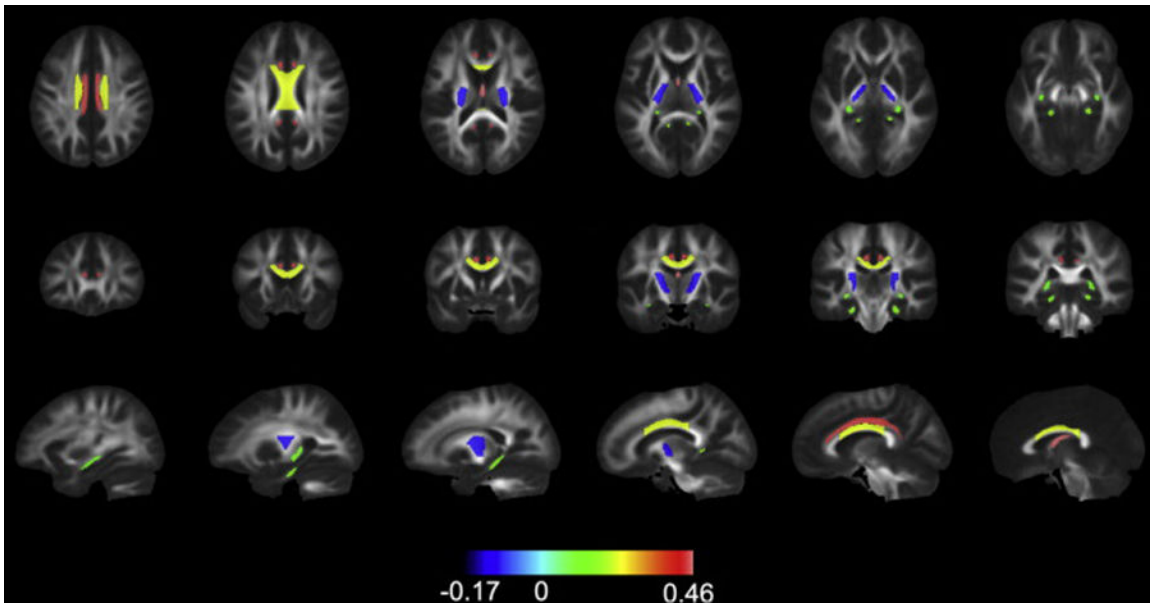

Fig 4.

Regional sensitivity to radiation. Tracts are filled with their corresponding coefficient for percent change in FA (from the model correlating mean dose to changes in the whole atlas ROI) and color coded according to value. Only statistically significant coefficients are shown. The signs for coefficients are flipped, i.e. FA is expected to decrease, so greater decreases in FA are represented by positive numbers and intensifying red color.

Table 1

Region of Interest Analysis of Dose Sensitivity: Linear mixed model coefficients (percent change per Gy) and p-values

Region of Interest	**FA**		**MD(× 10^{-6} mm^2/s)**		**$\lambda_{\parallel}$(× 10^{-6} mm^2/s)**		**$\lambda_{\perp}$(× 10^{-6} mm^2/s)**	
Dose	**Coefficient**	**p-value**	**Coefficient**	**p-value**	**Coefficient**	**p-value**	**Coefficient**	**p-value**
Anterior corona radiata								
Mean	−0.03	NS	**0.09**	**.007**	**0.07**	**.014**	0.10	.121
Max	−0.03	NS	**0.07**	**.001**	**0.06**	**.004**	**0.08**	**.030**
Anterior limb of internal capsule								
Mean	0.01	NS	**−0.08**	**.002**	−0.05	.117	**−0.11**	**.005**
Max	0.01	NS	**−0.06**	**.008**	−0.04	.235	**−0.08**	**.016**
Body of corpus callosum								
Mean	**−0.23**	**<.001**	**0.09**	**.016**	−0.05	NS	**0.27**	**<.001**
Max	**−0.16**	**<.001**	**0.07**	**.006**	−0.03	NS	**0.19**	**<.001**
Cingulum bundle								
Mean	**−0.44**	**<.001**	**0.12**	**<.001**	**−0.07**	**.003**	**0.28**	**<.001**
Max	**−0.32**	**<.001**	**0.09**	**<.001**	**−0.04**	**.025**	**0.21**	**<.001**
Cingulum (parahippocampal)								
Mean	**−0.16**	**<.001**	−0.03	NS	**−0.07**	**.008**	−0.01	NS
Max	**−0.12**	**<.001**	−0.01	NS	−0.04	.106	0.01	NS
Corticospinal tract								
Mean	−0.10	NS	−0.05	NS	−0.06	.472	−0.05	NS
Max	−0.07	NS	−0.03	NS	−0.03	NS	−0.03	NS
External capsule								
Mean	−0.02	NS	−0.01	NS	−0.01	NS	0.00	NS
Max	−0.01	NS	0.00	NS	0.00	NS	0.01	NS
Fornix (column and body of fornix)								
Mean	**−0.46**	**<.001**	**0.23**	**<.001**	0.04	NS	**0.40**	**<.001**
Max	**−0.40**	**<.001**	**0.20**	**<.001**	0.03	NS	**0.35**	**<.001**
Fornix (cres)/Stria terminalis								
Mean	**−0.11**	**.014**	−0.02	NS	**−0.08**	**<.001**	0.05	NS
Max	**−0.10**	**.005**	−0.01	NS	**−0.06**	**.001**	0.05	NS

Region of Interest	FA		MD(× 10^{-6} mm^2/s)		$\lambda_{\parallel}$(× 10^{-6} mm^2/s)		$\lambda_{\perp}$(× 10^{-6} mm^2/s)	
Dose	**Coefficient**	**p-value**	**Coefficient**	**p-value**	**Coefficient**	**p-value**	**Coefficient**	**p-value**
Genu of corpus callosum								
Mean	−0.12	.312	**0.10**	**.035**	0.04	NS	**0.16**	**.009**
Max	−0.09	.074	**0.07**	**.007**	0.02	NS	**0.13**	**<.001**
Posterior corona radiate								
Mean	0.03	NS	−0.02	NS	0.00	NS	−0.03	NS
Max	0.02	NS	0.00	NS	0.01	NS	−0.01	NS
Posterior limb of internal capsule								
Mean	**0.17**	**<.001**	**−0.08**	**.001**	0.02	NS	**−0.20**	**<.001**
Max	**0.13**	**<.001**	**−0.06**	**.010**	0.02	NS	**−0.14**	**<.001**
Posterior thalamic radiation								
Mean	−0.02	NS	−0.01	NS	−0.04	NS	0.03	NS
Max	−0.02	NS	0.00	NS	−0.02	NS	0.04	NS
Retrolenticular part of internal capsule								
Mean	0.08	.385	−0.03	NS	0.00	NS	−0.07	NS
Max	0.06	NS	−0.02	NS	0.00	NS	−0.05	NS
Sagittal stratum								
Mean	0.00	NS	−0.02	NS	−0.03	NS	−0.01	NS
Max	−0.01	NS	−0.01	NS	−0.02	NS	0.00	NS
Splenium								
Mean	−0.12	.054	0.07	.270	−0.02	NS	**0.17**	**<.001**
Max	**−0.10**	**.008**	**0.06**	**.039**	−0.01	NS	**0.14**	**<.001**
Superior corona radiate								
Mean	0.05	NS	−0.02	NS	0.01	NS	−0.06	NS
Max	0.04	NS	−0.01	NS	0.02	NS	−0.03	NS
Superior fronto-occipital fasciculus								
Mean	0.08	NS	**0.10**	**.001**	**0.10**	**<.001**	0.10	.075
Max	0.06	NS	**0.09**	**<.001**	**0.09**	**<.001**	**0.09**	**.025**
Superior longitudinal fasciculus								
Mean	−0.02	NS	−0.03	NS	−0.03	NS	−0.03	NS
Max	−0.02	NS	−0.02	NS	−0.02	NS	−0.01	NS

Region of Interest	FA		MD($\times 10^{-6}$ mm^2/s)		$\lambda_{\parallel}$($\times 10^{-6}$ mm^2/s)		$\lambda_{\perp}$($\times 10^{-6}$ mm^2/s)	
Dose	**Coefficient**	**p-value**	**Coefficient**	**p-value**	**Coefficient**	**p-value**	**Coefficient**	**p-value**
Tapetum								
Mean	−0.09	.384	**0.16**	**<.001**	**0.10**	**<.001**	**0.22**	**<.001**
Max	−0.09	.076	**0.15**	**<.001**	**0.09**	**<.001**	**0.20**	**<.001**
Uncinate fasciculus								
Mean	0.00	NS	−0.01	NS	−0.02	NS	0.01	NS
Max	0.00	NS	0.00	NS	−0.01	NS	0.02	NS

NS: p-values > 0.5 marked as "Not Significant"

Radiother Oncol. Author manuscript; available in PMC 2018 May 02.

Table 2

Skeletonized Tract Analysis of Dose Sensitivity: Linear mixed model coefficients (percent change per Gy) and p-values

TBSS Tract	**FA**		**MD(× 10^{-6} mm^2/s)**		**$\lambda_{\parallel}$(× 10^{-6} mm^2/s)**		**$\lambda_{\perp}$(× 10^{-6} mm^2/s)**	
Dose	**Coefficient**	**p-value**	**Coefficient**	**p-value**	**Coefficient**	**p-value**	**Coefficient**	**p-value**
Anterior corona radiata								
Mean	0.02	NS	0.02	NS	0.03	NS	0.01	NS
Max	0.01	NS	0.02	NS	0.02	NS	0.01	NS
Anterior limb of internal capsule								
Mean	0.06	.331	−0.04	.407	−0.01	NS	−0.08	.131
Max	0.05	.406	−0.03	NS	−0.01	NS	−0.06	.262
Body of corpus callosum								
Mean	−0.07	NS	0.01	NS	−0.04	NS	0.11	.089
Max	−0.05	NS	0.01	NS	−0.03	NS	**0.08**	**.034**
Cingulum bundle								
Mean	**−0.29**	**<.001**	**0.06**	**.007**	**−0.09**	**<.001**	**0.23**	**<.001**
Max	**−0.20**	**<.001**	**0.05**	**.001**	**−0.05**	**<.001**	**0.17**	**<.001**
Cingulum (parahippocampal)								
Mean	0.08	.135	**−0.09**	**<.001**	**−0.06**	**.005**	**−0.13**	**.001**
Max	0.06	.264	**−0.07**	**<.001**	**−0.04**	**.044**	**−0.09**	**.007**
Corticospinal tract								
Mean	−0.04	NS	−0.03	NS	−0.03	NS	−0.04	NS
Max	−0.02	NS	−0.01	NS	−0.01	NS	−0.02	NS
External capsule								
Mean	0.00	NS	−0.02	NS	−0.02	NS	−0.01	NS
Max	0.01	NS	−0.01	NS	−0.01	NS	−0.01	NS
Fornix (column and body of fornix)								
Mean	**−0.32**	**<.001**	**0.19**	**<.001**	0.03	NS	**0.35**	**<.001**
Max	**−0.26**	**<.001**	**0.16**	**<.001**	0.02	NS	**0.29**	**<.001**
Fornix (cres)/Stria terminalis								
Mean	−0.06	.303	**−0.08**	**<.001**	**−0.12**	**<.001**	−0.01	NS
Max	−0.06	.239	**−0.06**	**.002**	**−0.10**	**<.001**	0.00	NS

TBSS Tract	FA		MD(× 10^{-6} mm^2/s)		$\lambda_{\parallel}$(× 10^{-6} mm^2/s)		$\lambda_{\perp}$(× 10^{-6} mm^2/s)	
Dose	**Coefficient**	**p-value**	**Coefficient**	**p-value**	**Coefficient**	**p-value**	**Coefficient**	**p-value**
Genu of corpus callosum								
Mean	−0.01	NS	0.01	NS	0.00	NS	0.02	NS
Max	−0.02	NS	0.02	NS	0.00	NS	0.04	NS
Posterior corona radiate								
Mean	0.04	NS	−0.05	.478	−0.03	NS	−0.07	NS
Max	0.04	NS	−0.03	NS	−0.01	NS	−0.05	NS
Posterior limb of internal capsule								
Mean	**0.10**	**.002**	**−0.06**	**.002**	0.00	NS	**−0.17**	**<.001**
Max	**0.07**	**.004**	**−0.04**	**.024**	0.01	NS	**−0.12**	**<.001**
Posterior thalamic radiation								
Mean	−0.03	NS	−0.06	.087	**−0.09**	**<.001**	−0.01	NS
Max	−0.02	NS	−0.04	.235	**−0.06**	**.002**	0.00	NS
Retrolenticular part of internal capsule								
Mean	0.05	NS	−0.06	.052	−0.03	NS	−0.08	.090
Max	0.04	NS	−0.04	.108	−0.02	NS	−0.07	.123
Sagittal stratum								
Mean	0.01	NS	−0.05	.461	−0.05	.136	−0.04	NS
Max	0.01	NS	−0.04	NS	−0.04	.301	−0.02	NS
Splenium								
Mean	−0.01	NS	−0.03	NS	−0.04	NS	−0.02	NS
Max	−0.01	NS	−0.01	NS	−0.03	NS	0.01	NS
Superior corona radiate								
Mean	0.02	NS	−0.03	NS	−0.01	NS	−0.06	NS
Max	0.03	NS	−0.02	NS	0.01	NS	−0.04	NS
Superior fronto-occipital fasciculus								
Mean	0.07	NS	0.03	NS	0.04	NS	0.02	NS
Max	0.07	.161	0.03	NS	0.04	.173	0.02	NS
Superior longitudinal fasciculus								
Mean	0.00	NS	**−0.06**	**.048**	−0.05	.057	−0.07	NS
Max	0.00	NS	−0.04	.132	−0.03	.221	−0.05	NS

TBSS Tract	FA		MD($\times 10^{-6}$ mm^2/s)		$\lambda_{\parallel}$($\times 10^{-6}$ mm^2/s)		$\lambda_{\perp}$($\times 10^{-6}$ mm^2/s)	
Dose	**Coefficient**	**p-value**	**Coefficient**	**p-value**	**Coefficient**	**p-value**	**Coefficient**	**p-value**
Tapetum								
Mean	−0.03	NS	**0.08**	**.001**	**0.07**	**.008**	0.10	.101
Max	−0.02	NS	**0.08**	**<.001**	**0.06**	**.005**	**0.10**	**.030**
Uncinate fasciculus								
Mean	0.02	NS	−0.02	NS	−0.03	NS	0.00	NS
Max	0.02	NS	−0.02	NS	−0.02	NS	0.00	NS

NS: p-values > 0.5 marked as "Not Significant"